Structural and Thermodynamical Characterization of the Complete p21 Gene Product of Max†

Jean-François Naud,[§,‡] François-Olivier McDuff,[§] Simon Sauvé,[§] Martin Montagne,[§] Bradley A. Webb,[+] Steven P. Smith,[+] Benoit Chabot,[‡] and Pierre Lavigne*[,§]

Département de pharmacologie, Département de microbiologie et d'infectiologie, Faculté de médecine, Université de Sherbrooke, Sherbrooke, Quebec, Canada J1H 5N4, and Department of Biochemistry and Protein Function Discovery Group Queen's University, Kingston, Ontario, Canada K7L 3N6

Received January 13, 2005; Revised Manuscript Received May 30, 2005

ABSTRACT: The b-HLH-LZ family of transcription factors contains numerous proteins including the Myc and Mad families of proteins. Max heterodimerizes with other members to bind the E-Box DNA sequence in target gene promoters. Max is the only protein in this network that recognizes and binds E-Box DNA sequences as a homodimer in vitro and represses transcription of Myc target genes in vivo. Key information such as the structure of p21 Max, the complete gene product, and its K_D in the absence of DNA are still unknown. Here, we report the characterization of the secondary and quaternary structures, the dimerization and DNA binding of p21 Max and a thermodynamically stable mutant. The helical content of p21 Max indicates that its N-terminal and C-terminal regions are unstructured in the absence of DNA. NMR experiments further support the location of folded and unfolded domains. We also show that p21 Max has an apparent K_D (37 °C) of 7×10^{-6}, a value 10−100 times smaller than the b-HLH-LZ itself. We demonstrate that electrostatic repulsions are responsible for the higher K_D of the b-HLH-LZ. Finally, we show that a p21 Max double mutant forms a very stable dimer with a K_D (37 °C) of 3×10^{-10} and that the protein/DNA complex depicts a higher temperature of denaturation than p21 Max/DNA complex. Our results indicate that Max could homodimerize, bind DNA, and repress transcription in vivo and that its mutant could be more efficient at repressing the expression of c-Myc target genes.

The protein Max has been first discovered as a Myc interacting protein (*1*). It is the obligate partner of Myc (c-Myc, N-Myc, L-Myc) and Mad (Mad 1, Mxi 1, Mad 3, Mad 4) proteins. These proteins are all members of the b-HLH-LZ[1] family of transcription factors. The b-HLH-LZ domain mediates molecular recognition and DNA binding. As a heterodimer with the proteins of Myc family, Max can bind E-Box sequences (CACGTG) in promoters of Myc target genes, recruit protein complexes with histone acetyl transferase (HAT) activities or PTEFb complexes and activate transcription (*2*−*3*). The recruitment of co-activator proteins is mediated by the Myc Box I and II (MBI and MBII) in the transactivating domain. The c-Myc/Max heterodimer can also repress transcription through the interaction with Miz-1. This interaction is mediated by the HLH and the MBI and MBII domains of c-Myc and is independent of E-Box DNA binding (*4*−*7*). As a heterodimer with proteins of Mad family, Max can also bind E-Box sequences and recruit co-repressor complexes containing histone deacetylase (HDAC) activities. The mSin3 interacting domain (SID) on Mad proteins is responsible for the recruitment of these large complexes (*2*, *8*−*9*). While Max can bind E-Box sequences as a homodimer, it apparently lacks domains that actively recruit co-activators or co-repressors and is therefore thought to possess no transcriptional regulatory role as a homodimer. On the other hand, overexpression of Max can repress Myc target genes and limits cell proliferation (*10*−*11*). The mechanism by which this is achieved apparently involves a competition with endogenous c-Myc/Max heterodimers for E-Box DNA sequences in promoters of Myc target genes. Recently, Max and Mad proteins were shown to be upregulated by TGF-β (*12*). It is therefore suggested that Mad/Max heterodimers may play a major role in the mechanism responsible for the cytostatic effect of TGF-β. But, a transient repressor role for the Max homodimer cannot be ruled out given that the K_D of p21 Max and its solution structure in the absence of DNA are unknown. We have characterized the overall secondary and quaternary structures of p21 Max and p21 Max VL (N69V/H72L double mutation located in the LZ) and determined their apparent K_D to gain a better

† Grants (P.L. and B.C.) from the Canadian Institutes of Health Research (CIHR) supported this work. Pierre Lavigne acknowledges the Fonds de la Recherche en Santé du Québec (FRSQ) for a scholarship. Benoit Chabot is the recipient of a Canada Research Chair in Functional Genomics. Jean-François Naud is supported in part by Centre de Recherche Clinique (CRC) oncology group.

* All correspondence should be addressed to: Pierre Lavigne, Département de pharmacologie, Faculté de médecine, 3001 12e ave nord, Fleurimont, Québec, Canada J1H 5N4. Tel, 819-820-6868 ext. 15462; fax, 819-564-5400; e-mail, Pierre.Lavigne@USherbrooke.ca.

§ Département de pharmacologie, Université de Sherbrooke.

‡ Département de microbiologie et d'infectiologie, Université de Sherbrooke.

+ Department of Biochemistry and Protein Function Discovery Group Queen's University.

[1] Abbreviations: b-HLH-LZ, basic-Helix-Loop-Helix-Leucine Zipper; NMR, nuclear magnetic resonance; NLS, nuclear localisation sequence; HSQC, heteronuclear single quantum coherence spectroscopy; TROSY, transverse relaxation optimized spectroscopy.

10.1021/bi0500729 CCC: $30.25
Published on Web 09/02/2005

understanding of the molecular determinants dictating the homodimerization of Max. We determine by circular dichroism that the apparent K_D (37 °C) of p21 Max is 7×10^{-6}. Interestingly, the K_D of p21 Max is 10−100 times lower than the K_D (10^{-4}, 10^{-5}) for b-HLH-LZ domains. This indicates that the N- and C− terminal portions of p21 are involved in the stabilization of the homodimer. We provide evidence, both experimental and theoretical, suggesting that the stabilization of p21 Max homodimer by the N- and C-terminal regions is from electrostatic origin. We also show that the N69V/H72L double mutation in the LZ domain decreases the apparent K_D (37 °C) to 4×10^{-10} of p21 Max VL. Finally, we show that this increase in stability of p21 Max VL homodimer stimulates DNA complex formation. Altogether our results indicate that, at physiologically relevant concentrations, p21 Max can dimerize and bind DNA and that DNA binding can be improved by the stabilization of its LZ. Our results support a functional role for Max in the reversible repression of transcription of Myc target genes.

EXPERIMENTAL PROCEDURES

Construction of pET3a Expression Plasmid Encoding p21 Max and p21 Max VL. To obtain p21 Max, a polymerase chain reaction was performed using pVZ1 max (kindly provided by R. N. Eisenman, Fred Hutchinson Cancer Research Centre, Seattle, WA) as template. The 5′ and 3′ primers contained NdeI and BamHI restriction sites, respectively. The plasmid pET3a (Novagen) and PCR products were digested with the corresponding restriction enzymes and purified on an agarose gel using the QUIAquick gel extraction kit (Qiagen) before the ligation. The construct encoding p21 Max VL was obtained by site directed mutagenesis as described before (*13*).

Protein Expression and Purification. All proteins were prepared by induction of pET3a constructs in *Escherichia coli* with IPTG. The bacteria were grown either in LB or M9 media for the preparation of uniformly ^{15}N-labeled protein. In the later case, ^{12}C-glucose and $^{15}NH_4Cl$ were used as the sole source of carbon and nitrogen, respectively. The total protein extract was purified by cation-exchange chromatography. Briefly, after induction, cells were centrifuged at 4000 rpm in a Sorvall SLA-1500 rotor. The supernatant was discarded, and the pellet was resuspended in lysis buffer (50 mM Tris-HCl (pH 7.4), 0.1 M NaCl, 10 mM $MgCl_2$, and 0.1% NP-40). DNAse I was added, and the solution was incubated at 37 °C for 1 h. To precipitate DNA and acidic proteins, PEI was added and the solution was centrifuged at 20 000 rpm in a Sorvall SS34 for 30 min. The supernatant was kept, diluted in 5 vol of buffer A (50 mM sodium acetate (pH 5.0)), and loaded onto a HiTrap SP sepharose HP (Amersham Biotech) column preconditioned with buffer A. The column was washed with 5 vol of buffer B (50 mM sodium phosphate monobasic (pH 2.8) and 2 M urea). Elution of p21 Max and Max VL was achieved with a gradient of buffer C (50 mM sodium phosphate monobasic (pH 2.8), 2 M urea, and 3 M NaCl) from 0% to 100%. Fractions containing p21 Max WT and p21 Max VL were then desalted on HiTrap size-exclusion columns and lyophilized. The proteins were resuspended in phosphate buffer (50 mM sodium phosphate (pH 6.8) and 100 mM NaCl), and the concentrations of the stock samples were determined with Bio-Rad Protein Assay (Bio-Rad) and spectrophotometrically at 280 nm.

Circular Dichroism and Simulation of the Temperature Denaturation Curves. Circular dichroism measurements were performed on a Jasco J-810 spectropolarimeter equipped with a Jasco Peltier-type thermostat. The instrument was calibrated with an aqueous solution of d-10- (+)-camphor-sulfonic acid at 290.5 nm. Samples were loaded into quartz cells with a path length of 0.1 cm. Far-UV CD spectra were recorded at the desired temperature from 200 to 250 nm by averaging three scans at 0.1 nm intervals. The raw data were transformed in mean residue molar ellipticity ($[\theta]_{MRW}$, deg·cm^2·dmol^{-1}) using the following equation:

$$[\theta]_{MRW} = [\theta]\cdot MRW/c\cdot l\cdot 10 \quad (1)$$

where $[\theta]$ is in degree, MRW is the molecular weight divided by the number of residues, c is in g/mL, and l is in cm. Samples of proteins from the stock solutions were diluted to the desired concentration in 50 mM sodium phosphate (pH 6.8) and 100 mM KCl for p21 Max and p21 Max VL. Temperature-dependent denaturations were performed from 5 to 95 °C with a heating rate of 1 °C/min. The unfolding was recorded at 222 nm. For DNA studies, the dsDNA was created as described (*13*) and used at the desired concentration in 50 mM potassium phosphate (pH 6.8) and 100 mM KCl. For experiments made at different salt concentrations, the b-HLH-LZ of Max (Max*) was purified as described before (*13*). All proteins were diluted to a final concentration of 32 μM (in monomer unit), and thermal denaturations were recorded as before in 50 mM potassium phosphate (pH 6.8) with salt concentrations ranging from 0 to 500 mM KCl for Max* and 0−250 mM for p21 Max. The determination of the apparent K_D was performed by the simulation of the temperature denaturation curves with equations describing the equilibrium between a dimer and two monomers for p21 Max or between a dimer and two monomers with an intermediate state or p21 Max VL as described by Naud et al. (*13*). The calculated $[\theta]_{222}$ for a 151 amino acids α-helical protein was determined using the equation from Chen et al. (*14*).

NMR Spectroscopy. Uniformly ^{15}N-labeled proteins (p21 Max and p21 Max VL) were dissolve in 50 mM phosphate and 100 mM KCl containing 10% D_2O, DSS, and 50 mM NaN3 at pH 6.8 and approximately 1 mM concentration. All experiments were run on a Varian INOVA spectrometer operating at a ^{1}H frequency of 600 MHz and equipped with an indirect detection triple-resonance (^{1}H/^{13}C/^{15}N) probe with *Z*-axis pulsed-field gradients capability. The 2D ^{1}H-^{15}N-HSQC-TROSY (*15*, *16*) experiments for Max*VL and p21 Max VL were run at 45 °C. Spectra were collected with 152 transients of 768 data points and 200 $t1$ increment. The first increment of the ^{1}H-^{15}N-HSQC-TROSY of p21 Max was run at 35 °C with 10 000 transients of 768 data points, and those of Max*VL and p21 Max VL were run at 45 °C with 1000 and 10 000 transient of 768 data points, respectively. The 1D experiments were run at 35 °C with presaturation of the ^{1}H water resonance. All experiments were processed with NMRPipe (*17*) and analyzed with NMRView (*18*).

Analytical Ultracentrifugation. Samples used in analytical ultracentrifugation (AUC) were dialyzed extensively against

a)

```
                                  Basic Region          Helix 1          Loop      Helix 2
p21 Max      1   MSDNDDIEVE SDADKRAHHN ALERKRRDHI KDSFHSLRDS VPSLQGEKAS RAQILDKATE 60
p21 Max VL   1   MSDNDDIEVE SDADKRAHHN ALERKRRDHI KDSFHSLRDS VPSLQGEKAS RAQILDKATE 60
                                  Leucine Zipper
p21 Max      61  YIQYMRRKNH THQQDIDDLK RQNALLEQQV RALEKARSSA QLQTNYPSSD NSLYTNAKGS 120
p21 Max VL   61  YIQYMRRKVH TLQQDIDDLK RQNALLEQQV RALEKARSSA QLQTNYPSSD NSLYTNAKGS 120

p21 Max      121 TISAFDGGSD SSSESEPEEP QSRKKLRMEA S 151
p21 Max VL   121 TISAFDGGSD SSSESEPEEP QSRKKLRMEA S 151
```

b)

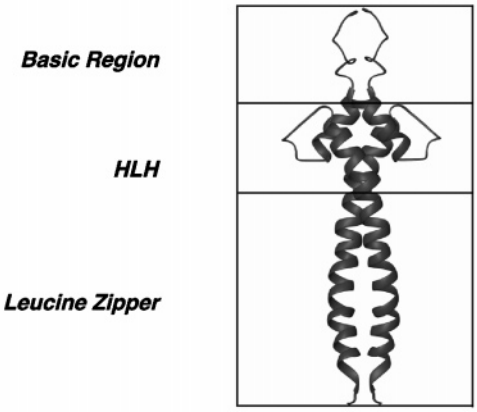

FIGURE 1: p21 Max and p21 Max VL recombinant proteins. (a) Amino acid sequences alignment of p21 Max and p21 Max VL. Amino acid sequences enclosed in box indicate the b-HLH-LZ domain of p21 Max and p21 Max VL and sequences outside the enclosed box, its N- and C-terminal ends. (b) Ribbons diagram of the NMR structure of the b-HLH-LZ of Max VL (1R05.pdb) in absence of DNA (*19*).

50 mM phosphate buffer (pH 6.8) and 100 mM KCl, which was saved and used in the reference sector for all runs. All AUC experiments were preformed at 20 °C. Sedimentation equilibrium analysis was preformed with a Beckman XL-I analytical ultracentrifuge with a four-hole An-60Ti rotor using 6-sector Epon charcoal centerpieces. Data were collected at 280 nm at 3 rotor speeds (15 000, 18 000, and 21 000 rpm) and at three protein concentrations (0.2, 0.4, and 0.6 mg/mL) for p21 Max p21 Max VL. Absorbance measurements were taken at 0.002 cm radial steps and averaged over 10 observations. Data sets were collected after equilibrium was obtained, as judged by the successive overlay of scans at 2-hour intervals. The partial specific volume and solution density were calculated using SEDNTERP (version 1.05, John Philo, 2000). The molecular weight for both a single ideal species and a monomer−dimer interaction were obtained using the XL-A/XL-I data analysis software (version 6.03, Beckman/Microcal).

The sedimentation velocity analyses were carried out at 20 °C in cells containing double-sector Epon charcoal centerpieces. Velocity runs for p21 Max and p21 Max VL were conducted at 50 000 rpm using Rayleigh interference optics. Interference scans were taken at intervals of 1 min for 400 scans. Best-fit profiles according to the continuous distribution c(S) Lamm equation model from SEDFIT (*19*) were overlaid on the experimental data using every second scan.

Molecular Modeling. Molecular modeling was performed on a SGI Octane 2 workstation using the Insight II suite (Accelerys). To generate the model for the folded p21 Max, the polypeptide chain corresponding to its primary structure was constructed in the extended state with the Biopolymer module. Residues corresponding to the folded domains of the b-HLH-LZ were template forced onto the structure of Max VL (1R05.pdb) (*20*) using the Discover module. We have subsequently run series of molecular dynamics simulations on the N- and C-terminal regions, while fixing the coordinates of the b-HLH-LZ, to randomize the dihedral angles of the extended form using the Discover module and the CVFF force field. The electrostatic potential maps were calculated with the Poisson−Boltzmann equation solver included in the program Grasp (*21*) using the default parameters and interpolated at the molecular surface at the same intensity to allow for relative comparison. All rendering were done with the program Ribbons (*22*).

RESULTS

The p21 Max Homodimer Is More Stable Than the b-HLH-LZ Homodimer, and Its LZ Domain Is Less Stable That Its HLH Domain. To characterize the secondary structure of p21 Max (Figure 1a), a far-UV circular dichroism (CD) spectrum was recorded at a concentration of 32 μM (monomer units), pH 6.8, and 20 °C (Figure 2a). p21 Max has the typical CD spectrum expected for a mixture of random coil and α-helix. This is further supported by the isodichroic point observed at 203 nm indicating that p21 Max has only α-helical structure and random coil without significant contribution of β-sheet (data not shown). The isodichroic point is obtained by superimposition of the CD spectra at different temperatures. According to the equation of Chen et al. (*14*), the theoretical mean residue molar ellipticity at 222 nm ($[\theta]_{222}$) expected for a protein of 151 amino acids 100% α-helical

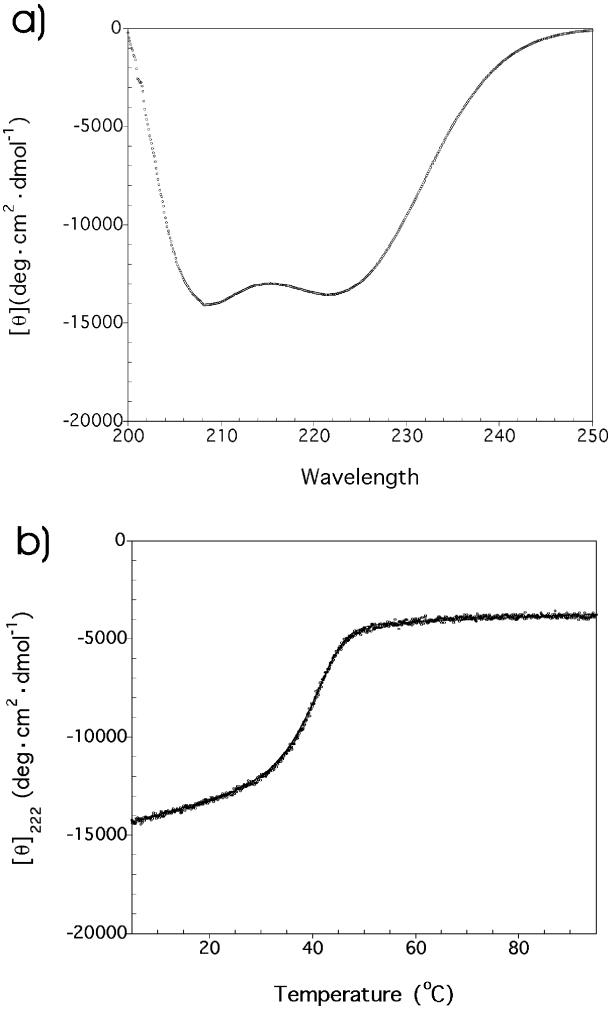

FIGURE 2: Far-UV CD spectra (a) and temperature-induced denaturation (b) of p21 Max. Spectra are presented in units of mean residue ellipticity ([θ]). The unfolding reaction was monitored by recording [θ] at 222 nm as function of temperature. Denaturation was found to be fully reversible. Proteins samples were at a concentration of 32 μM (monomer units) in 50 mM phosphate (pH 6.8) and 100 mM KCl. The continuous line shows the best-fit of the data with eq 1 (see Experimental Procedures). The best-fit parameters are listed in Table 1.

is $-38\,400$ deg·cm^2·dmol^{-1}. The $[\theta]_{222}$ observed for p21 Max is $-13\,200$ deg·cm^2·dmol^{-1}, indicating that the equivalent of 34% or 52 residues are α-helical in the absence of DNA. As reported elsewhere, the basic region of b-HLH-LZ of Max is mostly unfolded in the absence of DNA (*13*, *20*), with only the last four residues being helical (*20*). It can be calculated that if the LZ, H1, and H2 domains were fully helical, plus the four residues of the basic region, this would amount to 60 residues or a $[\theta]_{222}$ of approximately $-16\,000$ deg·cm^2·dmol^{-1}. Hence, it appears that, under these conditions, the N- and C-termini of p21 Max are random coil, and that p21 Max exists as either a 86% population of a dimer with a b-HLH-LZ optimally folded or a 100% population of a dimer with 14% of the b-HLH-LZ unfolded. To further explore this aspect and to determine the apparent K_D of the p21 Max, we recorded its thermal denaturation by monitoring the molar ellipticity at 222 nm as a function of temperature. On the basis of the sedimentation equilibrium analysis result (see below and Figure 3a), denaturation curve was simulated with a thermodynamical model consisting of a two-state reaction of dimer dissociation coupled to the unfolding of monomers, as described in details in Naud et al. (*13*) (Figure 2b). We initially tried, without success, to simulate the denaturation using a baseline for the folded state having $[\theta]_{222}$ values around $-16\,000$ deg·cm^2·dmol^{-1} corresponding to an optimally folded b-HLH-LZ. This suggests that p21 Max is a partially folded dimer having 86% of the optimal ellipticity of the b-HLH-LZ at room temperature. Indeed, we could fit the denaturation with values for the native state of $-14\,700$ deg·cm^2·dmol^{-1}, and from this simulation we could determine an apparent K_D (20 °C) of 6.5×10^{-9}, which corresponds to a population of 99% of the dimeric state at 32 μM. The apparent K_D (37 °C) is 7.2×10^{-6}, and the corresponding $\Delta G_D°$ (37 °C), $\Delta H_D°$ (37 °C), and $T°\Delta S_D°$ (37 °C) were 7.3 kcal·mol^{-1}, 83.15 kcal·mol^{-1}, and 78.85 kcal·mol^{-1}, respectively (Table 1). The $\Delta G°$ (T), $\Delta H°$ (T), $T·\Delta S°$ (T), and the population plots can be found in Supporting Information. The analysis of the crystallographic structure in the presence of DNA reveals that LZ of p21 Max is not well-ordered, supporting our CD data and indicating that the dimeric b-HLH-LZ of p21 Max is only partially folded with the LZ domain undergoing a microscopic reversible folding−unfolding transition within macroscopic-folded dimeric state (*23*). This is supported by the fact that the LZ in the crystal structure of the b-HLH-LZ domain of Max also frays toward its C-terminal end (*24*). Furthermore, proteolysis of Max b-HLH-LZ has shown that the LZ domain was more susceptible to cleavage by many endoproteases than the HLH (*24*), indicating that LZ is less thermodynamically stable (*13*). Taken together, our data strongly suggest that the N- and C-terminal flanking regions of the b-HLH-LZ of p21 Max are unfolded and that p21 Max is a b-HLH-LZ dimer with an unstable LZ domain. Finally, the K_D observed for p21 Max (7.2×10^{-6}) is lower than the K_D reported for the b-HLH-LZ (10×10^{-5}) (*13*, *26*). Interestingly, lower K_Ds were reported for the b-HLH-LZ domain by Krylov et al. with a K_D (37 °C) of 6×10^{-6} (*27*). On the other hand, it is important to notice that their temperature denaturations were done at higher KCl concentration and pH than in our experiments. As described below, salt concentration has a profound effect on the stability of Max b-HLH-LZ. In addition, the Max b-HLH-LZ stability is very sensitive to pH around 7 with His72 located directly at the interface. Considering a generic pK_a of 6.5, the protonation state of His72 will change drastically from 6.8 to 7.4 and will become mostly neutral at the latter pH. Protonation of His72 has been shown to be very destabilizing and enough to unfold the LZ domain at low pH (*13*). Accordingly, others (*26*) and we (data not shown) have observed that increasing the pH from 6 to 8 significantly stabilizes the Max b-HLH-LZ homodimer explaining why our reported value is slightly higher than the one previously reported by Krylov et al. However, the K_D of p21 Max is similar to that obtained by Horiuchi et al. (8×10^{-6}) for a truncated Max (p110) containing the first 110 amino acids and determined at pH 6.8 (*28*).

So far, our structural and thermodynamical characterization indicates that the LZ of p21 Max is most likely fraying and that the N-terminal and possibly the C-terminal portions could influence the dissociation constant of the protein even though they are not structured. As described below, evidence

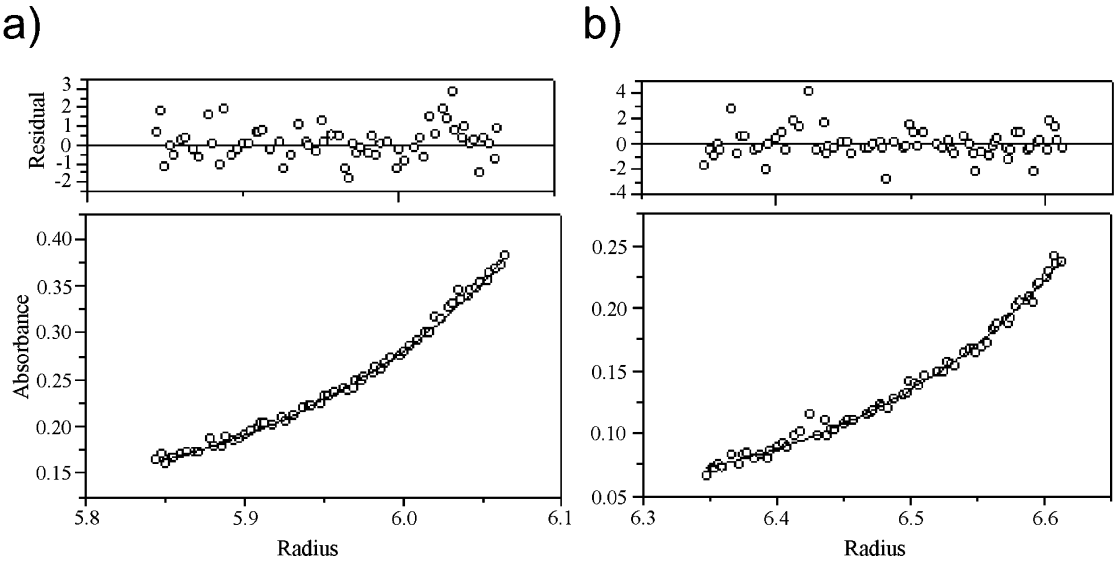

FIGURE 3: Analysis of the oligomeric solution state of p21 Max and p21 Max VL by sedimentation equilibrium analysis. Panels (a) and (b) show the residual and absorbance plots from the sedimentation equilibrium run of p21 Max and p21 Max VL. Open circles show the UV absorbance gradient in the centrifuge cell. The data were fitted to a monomer−dimer equilibrium, and the solid line denotes the fitted curve calculated from three rotor speeds and multiple protein concentrations. As judged from the goodness of the fits, both p21 Max and p21 Max VL are dimeric. Residuals show the difference in the fitted and experimental values as a function of radial position.

Table 1: Thermodynamic Parameters Obtained from the Fitting of the Temperature-Induced Denaturation as Described in Experimental Procedures[a]

p21 Max		p21 Max VL	
$T_D°$	41.6 °C	$T_I°$	58.2 °C
		$T_D°$	67.5 °C
ΔG_D (37 °C)	7.30 kcal/mol	ΔG_I (37 °C)	4.09 kcal/mol
		ΔG_D (37 °C)	13.50 kcal/mol
ΔH_D (37 °C)	83.15 kcal/mol	ΔH_I (37 °C)	59.75 kcal/mol
		ΔH_D (37 °C)	68.35 kcal/mol
ΔS_D (37 °C)	0.244 kcal/(mol·K)	ΔS_I (37 °C)	0.179 kcal/(mol·K)
		ΔS_D (37 °C)	0.177 kcal/(mol·K)
K_D(37 °C)	7.16×10^{-6}	K_I (37 °C)	1.32×10^{-3}
		K_D (37 °C)	3.09×10^{-10}

[a] For p21 Max and p21 Max VL, thermodynamic parameters of unfolding are indicated by the letter D. Thermodynamic parameters for the intermediate state present during the unfolding of p21 Max VL are also shown (identified by the letter I).

leads to suggest that this effect might be from electrostatic origins.

The N69V/H72L Mutations Promote the Folding of the LZ Domain and Improve the Stability of the p21 Max Dimer. To verify the hypothesis that the LZ domain of p21 Max is undergoing unfolding−folding reaction in its dimeric state, we have proceeded to a double mutation (N69V and H72L) targeted at stabilizing the LZ domain. Residues N69a and H72d in the LZ domain of p21 Max have been proposed to be key determinants in the molecular recognition of Max with the Myc and Mad proteins by promoting the dissociation of homodimers and encouraging specific interactions at the interface of heterodimers (e.g., c-Myc/Max and Mad1/Max) (*29*−*31*). Mutation of these two residues in the b-HLH-LZ domain of Max dramatically increases thermodynamic stability of the LZ and the b-HLH-LZ homodimers (*13*). This increase in stability was accompanied by an increase in α-helical content that matches the expected one for a fully folded HLH-LZ. Therefore, if the LZ domain of p21 Max is fraying, this double mutation should increase the thermodynamical stability and increase the helical content to that expected for a fully folded LZ domain. To verify the effect of these mutations on the secondary and quaternary structures of the complete gene product, we have made p21 Max VL (Figure 1a) and characterized it by CD as described in the previous section for p21 Max. The CD spectrum obtained at pH 6.8 and 20 °C is typical of a mixture between random coil and α-helical structures (Figure 4a). The $[\theta]_{222}$ of p21 Max is − 16 600 deg·cm^2·dmol^{-1}, indicating that the α-helical content of the double mutant is nearly 43% or equivalent to 65 residues folded in an α-helical conformation. Recently, the solution-NMR structure of the b-HLH-LZ bearing the same double mutation has been solved (*20*). Residues from R27 in the b-region to V41 in the H1 and residues from R51 in H2 to E94 in LZ (Figure 1a) were found to be in a α-helical conformation. These amount to 60 residues, a figure close to the 65 residues estimated from the CD spectrum. This strongly suggests that part of the b region, H1, H2, and LZ of p21 Max VL are α-helical and that the missing α-helical content of p21 Max is located in the LZ domains. To estimate the K_D (37 °C) of p21 Max VL, we have performed thermal denaturation (Figure 4b). The denaturation curve could not be simulated by a simple two-state denaturation reaction like p21 Max. This indicates that an intermediate state is populated and confirms previous results obtained with the b-HLH-LZ (*13*). The intermediate state corresponds to a dimeric state where the LZ is folded while the HLH is unfolded. The dimeric state of p21 Max was verified by sedimentation equilibrium analysis to ensure that the double mutation did not promote oligomerization as described below (Figure 3b). In Figure 4b, we show the simulation of the denaturation curve according to this model by a solid line. The thermodynamical parameters obtained from the simulation are summarized in Table 1. The $\Delta G_I°$ (37 °C), $\Delta H_I°$ (37 °C), and $\Delta S_I°$ (37 °C) for the transition between the native and the intermediate dimeric state were found to be equal to 4.1 kcal·mol^{-1}, 59.8 kcal·mol^{-1}, and 55.7 kcal·mol^{-1}, respectively. The $\Delta G_D°$ (37 °C), $\Delta H_D°$ (37

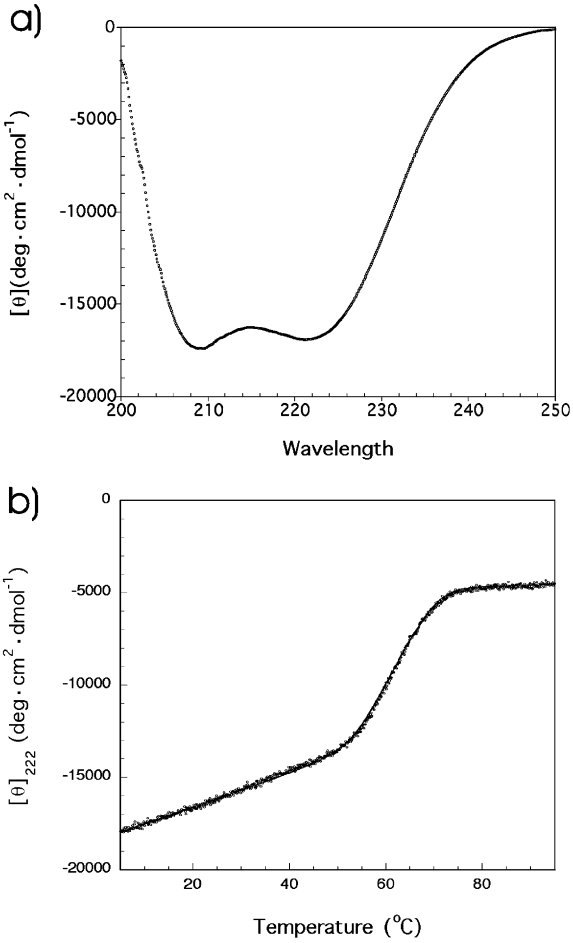

FIGURE 4: Far-UV CD spectra (a) and temperature-induced denaturation (b) of p21 Max VL. Spectra are presented in units of mean residue ellipticity ([θ]). The unfolding reaction was monitored by recording [θ] at 222 nm as a function of temperature. Denaturation was found to be fully reversible. Proteins samples were at a concentration of 32 μM (monomer units) in 50 mM phosphate (pH 6.8) and 100 mM KCl. The continuous line shows the best-fit of the data (see details in Experimental Procedures). The best-fit parameters are listed in Table 2.

°C), and $\Delta S_D°$ (37 °C) for the transition between the native dimeric state and the unfolded monomeric state were found to be equal to 13.5 kcal·mol^{-1}, 68.3 kcal·mol^{-1}, and 54.9 kcal·mol^{-1}, respectively. The corresponding $\Delta G°$ (T), $\Delta H°$ (T), and $T·\Delta S°$ (T) plots can be found in the Supporting Information. The $\Delta G_D°$ (37 °C) indicates a K_D (37 °C) of p21 Max VL that is 10 000-fold lower than the value of p21 Max (3×10^{-10}). These results support that the LZ domain of p21 Max is fraying in its dimeric state and that residues N69a and H72d are key determinants for the destabilization of p21 Max and its reversible dimerization.

Assertion of the Dimeric State of p21 Max and p21 Max VL by Sedimentation Equilibrium and Velocity Analytical Ultracentrifugation. To assess the impact of the mutation on the oligomeric state of p21 Max, we used sedimentation equilibrium and velocity analytical ultracentrifugation (AUC). When the sedimentation equilibrium AUC data were fitted to a single species model, the apparent weight-average molecular masses of p21 Max and p21 Max VL were approximately 39 kDa and 34 kDa (Table 2, Figure 3, parts a,b), respectively, and this suggests that the N69V/H72L double mutation has not impact on the oligomeric state of

Table 2: Molecular Masses and Hydrodynamics Properties of p21 Max and p21 Max VL[a]

	SE	SV		
construct (kDa)	M_r (kDa)	S	f/f_o	M_r (kDa)
WT (34.4)	39.5	2.33	1.5	30.5
VL (34.3)	34.9	2.24	1.69	34.1

[a] See text for details.

p21 Max. Sedimentation velocity experiments were also performed to examine the hydrodynamic properties of p21 Max and p21 Max VL. Sedimentation profiles were evaluated by a continuous distribution c(S) Lamm equation model. When the sedimentation coefficient distribution was determined, major peaks of 2.33 and 2.24 S corresponding to molecular masses of approximately 30.5 and 34.1 kDa, for p21 Max and p21 Max VL, respectively, were revealed. Furthermore, in both cases, no higher order oligomers were observed. The velocity data was also exploited to crudely model the shape of p21 Max and p21 Max VL constructs. Frictional ratios, f/f_o, of 1.5 and 1.69 were calculated for the two constructs. This implies that both p21 Max and p21 Max VL adopt asymmetric/elongated shapes in solution. This is in agreement with the solution structure of Max*VL. Indeed, we have shown that Max*VL undergoes severe rotational diffusion anisotropy and behaves as an axially symmetrical prolate ellipsoid with an anisotropy ratio of approximately 2 (*20*). Interestingly, the f/f_o of p21 Max VL is 10% larger than that of p21 Max, indicating that, hydrodynamically, p21 Max VL appears more asymmetric/elongated than p21 Max. This is expected for p21 Max if its LZ domain undergoes a microscopic folding−unfolding transition. Because the LZ domain of p21 Max VL is stabilized, the shape adopted by p21 Max VL in solution will be, on a time average, more elongated. Thus, the sedimentation equilibrium and velocity experiments show that p21 Max and p21 Max VL proteins are both dimers, that p21 Max is less asymmetrical at the concentrations analyzed, and that p21 Max constructs have the same shape in solution.

Localization of the Secondary Structure on p21 Max and p21 Max VL by NMR. Although the helical content and K_D suggest that both p21 Max and p21 Max VL have the HLH and LZ domains folded and that the other regions of the proteins are unfolded, it is important to confirm the exact location of the α-helical secondary structure. Therefore, specific and spectroscopic markers proving that LZ and HLH domains are folded need to be provided. In that regard, during the assignment of the ^{1}H, ^{13}C, and ^{15}N resonances (BioMagResBank accession number BMRB-5926) of Max*VL, we have noticed that the δ-methyl ^{1}H of L55 were upfield-shifted by a ring current effect from F34 (*20*). Indeed, the structure shows that the side chain of L55 packs against the phenyl ring of F34 in the middle of the folded HLH hydrophobic core. In Figure 5a, the upfield region of the Max*VL ^{1}H-1D spectra is displayed and the shielded ^{1}H-methyl of L55 are depicted. Other upfield-shifted ^{1}H-methyl resonances belonging to the HLH are also labeled (*L37, V41, L44*). If the HLH domains of p21 Max and p21 MaxVL are similarly folded, the same resonances should be observed on their ^{1}H-1D spectra. This is the case for both p21 Max (Figure 5b) and p21 Max VL (Figure 5c). As expected from the increased

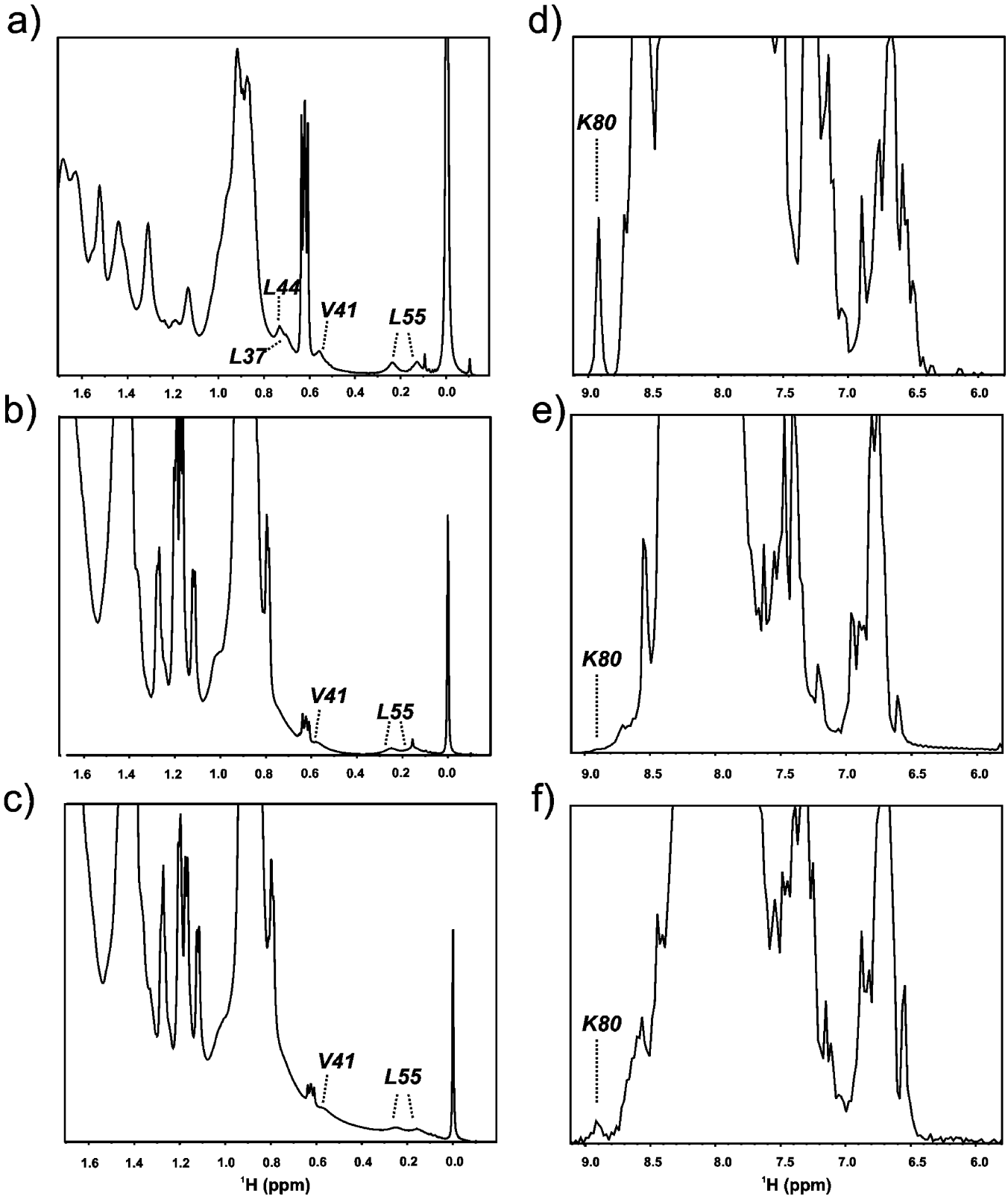

FIGURE 5: NMR evidence that the HLH of the complete gene product is folded and that the LZ of p21 Max in undergoing a dynamical process. The upfield regions of the ^{1}H-1D spectra of Max*VL (a), p21 Max (b), and p21 Max VL (c) are displayed, and the ^{1}H-methyl resonances located in the folded HLH are labeled. The first increments of the ^{1}H-^{15}N-HSQC-TROSY spectra of Max*VL (d), p21 Max (e), and p21 Max VL (f) are depicted, and the resonance of the backbone ^{1}HN of K80, which serves as a probe for the folded LZ domain, is labeled.

molecular weight of the complete gene product constructs, the resonances of p21 Max and p21 Max VL are markedly broader in respect to Max*VL. This is due by an increase in overall rotational correlation time and consequent decrease in T_2, which naturally leads to the line-broadening observed. Nevertheless, the same spectroscopic and domain-specific markers are present and confirm the fact that the HLH domains of p21 Max and p21 Max VL are stably folded.

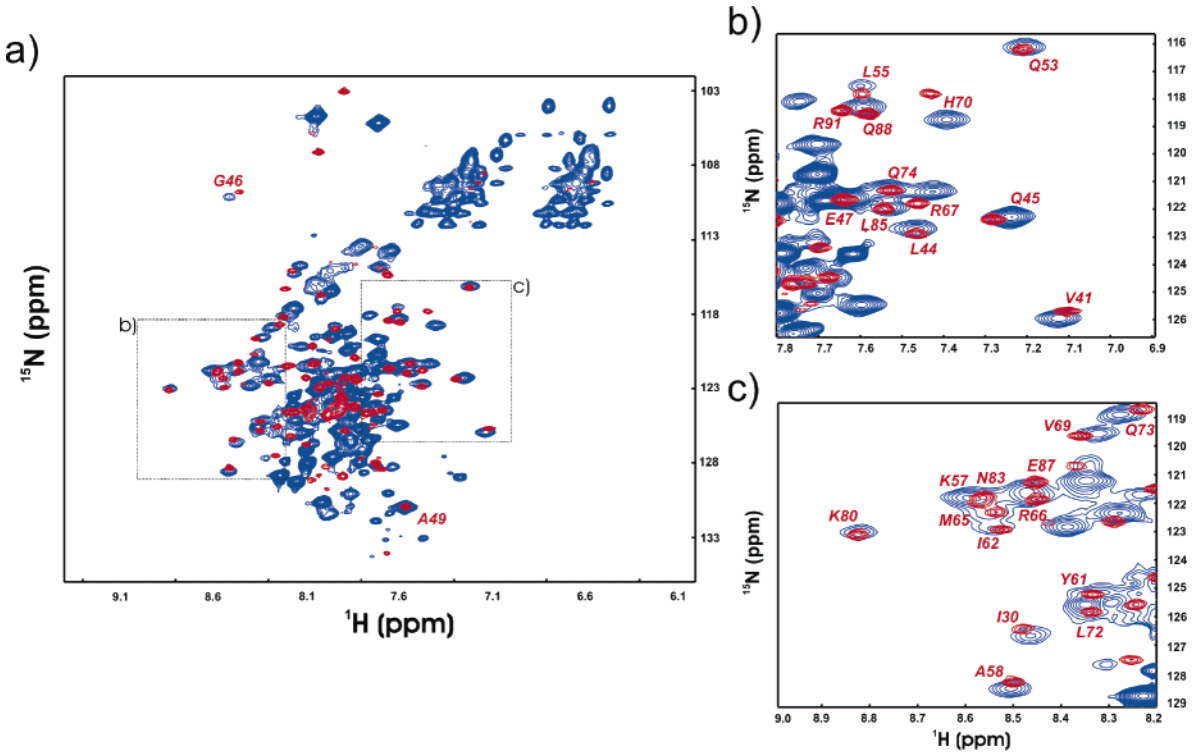

FIGURE 6: Localization of the α-helical secondary structure in the LZ and HLH domains for the complete gene product. Superimposition of the ^{1}H-^{15}N-HSQC-TROSY spectra of Max*VL (red) and p21 MaxVL (blue) suggests that the LZ and HLH of p21 Max VL are stably folded and α-helical. Regions depicting many of the resonances belonging to the HLH (b) and the LZ (c) are enlarged, and residues located in the different folded and α-helical domains of Max*VL are labeled.

To further confirm the folded nature of HLH-LZ in the p21 constructs and the dynamical folded nature of the LZ domain in the case of p21 Max, we have recorded their ^{1}H-^{15}N-HSQC-TROSY spectra (*32*) and compared them to the spectrum of Max*VL (Figure 6a). ^{1}H-^{15}N-HSQC spectra informs on the folded nature of proteins and the local magnetic environment of backbone (and side chain) ^{1}H−^{15}N spin pairs. Therefore, if the folded regions of the different constructs are similar, the magnetic environment of the folded backbone ^{1}H−^{15}N pairs should also be similar. Thus, the resonance frequencies of ^{1}H−^{15}N cross-peaks assigned to the LZ and HLH of Max*VL should appear in the spectra of the complete gene product. In Figure 6, the ^{1}H-^{15}N-HSQC-TROSY spectrum of Max*VL (red) is superimposed onto the spectrum of p21 Max VL (blue). As expected, many assigned cross-peaks from the HLH domain of Max*VL have corresponding cross-peak in the p21 Max VL spectrum (V41, G46, and Q53; Figure 6b) indicating that the HLH is similarly folded as inferred above from the presence of the two upfield-shifted methyl resonances. Similarly, one can also note that many ^{1}HN downfield cross-peaks, which correspond to the LZ domain, are found in p21 Max VL. In α-helical proteins containing LZ domains, downfield backbone ^{1}HN are usually involved in strong main-chain H-bonds and are located at the buried interface (e.g., K80 and N72). Although the environment of the ^{1}H−^{15}N pair may not be exactly identical, we believe that it is reasonable to propose that the HLH-LZ of both p21 Max VL and Max*VL are similarly and stably folded.

From Figure 6, one can also notice the obvious increase in line widths of the cross-peaks of p21 MaxVL compared to those of Max*VL. It is noteworthy to report that the average ^{15}N-T_2 values of Max*VL are of the order of 30 ms (*20*). These are rather short and gave rise to broad line widths for a protein the size of Max*VL (20 kDa). They represent ^{15}N-T_2 values a globular protein almost twice that size would have. This was rationalized by the severe rotational diffusion anisotropy of Max*VL as discussed above. Considering that the MW of p21 Max is almost twice the MW of Max*VL, it is to be expected the ^{15}N-T_2 of p21 Max will be markedly decreased and that the half-width at half-height (HWHH) of the resonances will be increased (*33*). Interestingly, the ^{1}H-^{15}N-HSQC-TROSY of p21 Max only showed well-resolved resonances belonging to the HLH (data not shown). We remind that the LZ domain of this construct is expected to undergo a microscopic folding−unfolding transition. This exchange phenomenon usually occurs on the millisecond time scale, which can broaden the line width of resonances beyond detection (*34*). To illustrate the existence of a dynamical phenomenon in the LZ domain of p21 Max, we show, in Figure 5, the first increment of the ^{1}H-^{15}N-HSQC-TROSY spectra of Max*VL (Figure 5d), p21 Max (Figure 5e), and p21 Max VL (Figure 5f). One can see that the resonance of K80, which is located in the middle of the LZ domain and buried at the interface, is sharp in the spectrum of Max*VL (Figure 5d). In accordance with the above discussion, the resonance of K80 is significantly broader (larger HWHH) in the spectrum of p21 Max VL (Figure 5f) and is broadened almost beyond detection in the p21 Max spectrum (Figure 5e). Taken as a whole, the NMR and CD results presented so far support the fact that the helical content of both p21 Max VL and p21 Max, in its dynamically populated and fully folded state, is located in the HLH-LZ and that the N- and C-termini are essentially unfolded.

The N- and C-terminal portions of p21 Max relieve electrostatic repulsions present in the b-HLH-LZ.

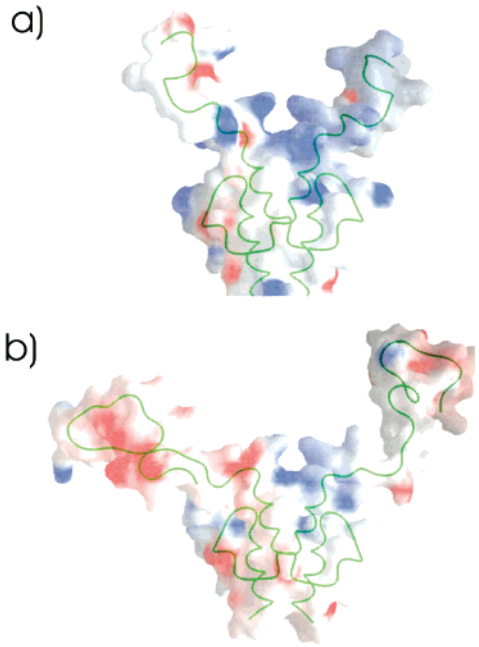

FIGURE 7: The electrostatic potential interpolated at the molecular surface of Max*VL (a) and a model of p21 Max (b). The blue and red colors represent positive and negative potential, respectively. The electrostatic potential maps were calculated using the Poisson−Boltzmann equation solver included in the program Grasp (*17*) using the default parameters and interpolated at the molecular surface at the same level. Note the darker blue color (positive electrostatic potential) at the interface of the HLH of Max*VL.

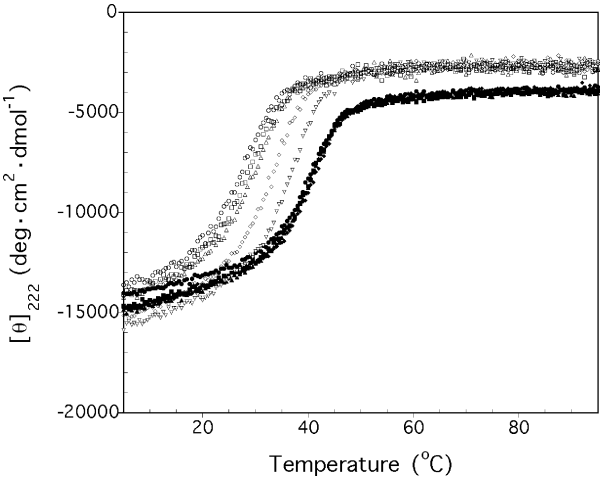

FIGURE 8: Temperature-induced denaturations of (empty symbols) b-HLH-LZ of Max and (fill symbols) p21 Max in 50 mM phosphate buffer (pH6.8) with concentration of KCl from 0 mM (circle), 50 mM (square), 100 mM (triangle), and 250 mM (diamond). For the b-HLH-LZ of Max, an additional denaturation in 50 mM phosphate buffer (pH6.8) with concentration of 500 mM KCl (reverse triangle) was done. All denaturations were done at protein concentration of 32 μM.

As alluded to above, evidence suggests that the lower thermodynamical stability of the b-HLH-LZ compared to the complete is of electrostatic origin. Indeed, we have shown the existence of a cluster of positively charged side chains at the interface of the HLH in the solution structure of the dimeric b-HLH-LZ of Max (*20*). This cluster generates high local electrostatic potential that induces significant molecular motions in the helix 1 of the HLH on the nanosecond time scale. We show in Figure 7a, the b-HLH of Max* with the electrostatic potential interpolated at its molecular surface and displaying a net positive (blue) electrostatic potential. It is straightforward to propose that repulsions may destabilize the HLH and promote unfolding. On the other hand, what are the roles of the N- and/or C-terminal regions in stabilizing the dimeric form of the complete gene product? Interestingly, the p*I*s of Max b-HLH-LZ, p110, and p21 Max are 9.69, 6.29, and 6.07, respectively. In fact, one can see in Figure 1, that the N-terminal region of Max is rich in acidic residues, explaining the decrease in p*I* of p110 and the complete gene product. When the electrostatic potential is calculated and interpolated at the molecular surface of the b-HLH-LZ of p21 Max with an unfolded N-terminal region, it is apparent that the latter reduces significantly the net positive electrostatic potential at the interface of the b-HLH (Figure 7b). It is therefore possible that the N-terminus, even unstructured, could reduce the unfavorable electrostatic repulsions at the interface of the HLH in p21 Max, leading to a smaller K_D or an increased thermodynamical stability.

To further test this hypothesis, temperature-induced denaturations were recorded with the b-HLH-LZ of Max and p21 Max at 32 μM in 50 mM phosphate buffer (pH 6.8) at different ionic strengths (0−500 mM KCl) to screen for the contribution of electrostatic repulsions (Figure 8). At 100 mM KCl and below 20 °C, the molar ellipticites and α-helical content of the b-HLH-LZ and p21 Max are comparable, confirming that the dimers are folded similarly. However, the stability of p21 Max is insensitive to ionic strength, while that of the b-HLH-LZ is largely increased by the ionic strength. This strongly supports our suggestion that electrostatic repulsions are present in the b-HLH-LZ and that the N- and C-terminal portions are lowering the K_D (increasing stability) of p21 Max by decreasing the destabilizing effect repulsions at the interface of the HLH in the complete gene product.

p21 Max VL Forms a More Stable Protein/DNA Complex Than p21 Max. As discussed in the Introduction, in light of a possible function of Max in the repression of the transcription of Myc target genes in cancer cells, an increase of the stability of its complex with E-Box sequences would be advantageous. It can be envisaged that an increase in the stability of the dimeric form of p21 Max by the double mutation could result in an increased stability of its specific DNA complex. To address the impact of the stabilization of p21 Max VL on the stability of the respective E-Box/DNA complexes, we recorded the temperature-induced denaturations monitored by CD of p21 Max and p21 Max VL in the presence of an E-box dsDNA at a protein/DNA ratio of 1:1 and 32 μM (Figure 9). At 20 °C, the K_D of both p21 Max and p21 Max VL were below 10^{-9}, indicating that the population of dimeric species at 20 °C and 32 μM was 100% in both cases (Supporting Information). As can be seen in Figure 9, the two curves suggest a two-state process in accord with temperature-induced DNA dissociation followed by the coupled dissociation/unfolding of p21 Max. The melting curve for the E-Box dsDNA has been reported elsewhere and has been subtracted from the raw denaturation curves. The $T°$ of E-Box dsDNA is 75 °C, a value above both apparent denaturation $T°$ for the p21 Max (42 °C) and p21 Max VL (67 °C). As reported previously by several groups, the α-helical content of the dimeric b-HLH-LZ of Max is increased in the presence of E-Box dsDNA. This improve-

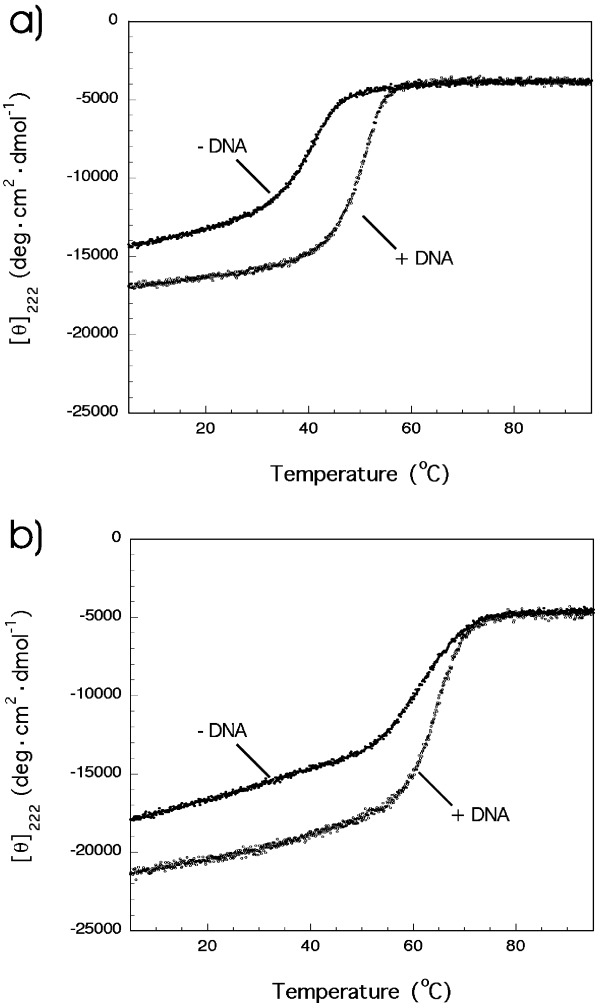

FIGURE 9: Temperature-induced denaturations on p21 Max and p21 Max VL with (empty circles) and without (fill symbols) E-Box dsDNA. The protein and E-Box dsDNA are at concentration of 32 μM (monomer units) and dissolved in 50 mM phosphate buffer (pH 6.8) and 100 mM KCl.

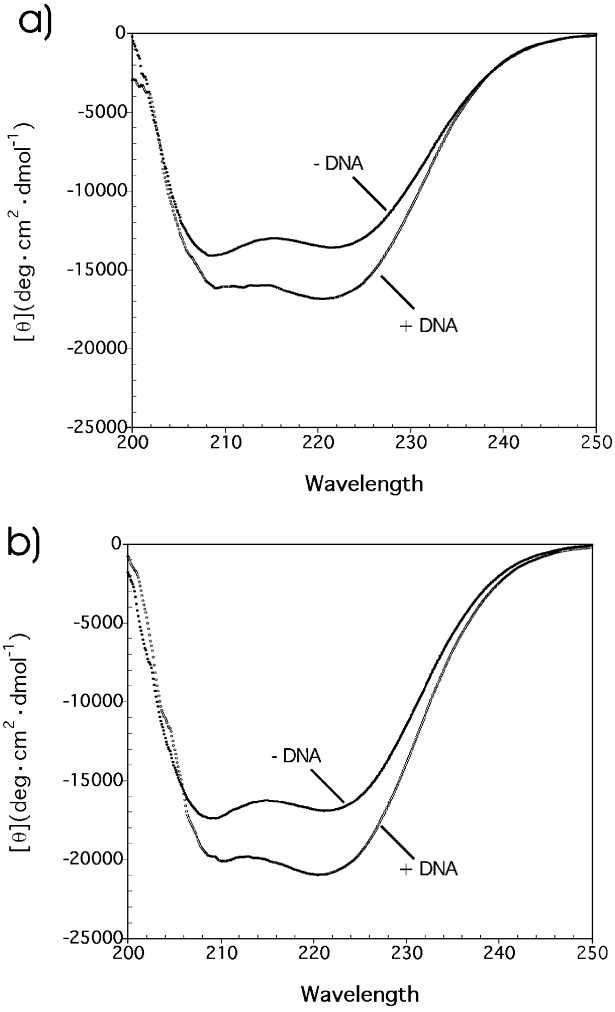

FIGURE 10: Far-UV CD spectra of (a) p21 Max and (b) p21 Max VL with (empty circles) and without (fill circles) E-Box dsDNA. The proteins and E-Box dsDNA are at concentration of 32 μM (monomer units) and dissolved in 50 mM phosphate buffer (pH 6.8) and 100 mM KCl.

ment was attributed to the folding/stabilization of the b-region by DNA (*13*, *28*). The [θ] values at 222 nm of both p21 Max and p21 Max VL are increased in the presence of E-Box dsDNA by 3003 and 3698 deg·cm^2·dmol^{-1}, respectively, as it can be seen in far-UV CD spectra at 32 μM, pH 6.8, and 20 °C (Figure 10). The gain in [θ] at 222 nm of 3003 and 3698 deg·cm^2·dmol^{-1} corresponds to the folding of 12 to 14 residues, respectively, into α-helical structure, a value in accord with the folding/stabilization of the b-region induced by DNA binding. As judged from the relative increase in the apparent T°, it can also be observed that DNA binding results in a larger gain in stability for p21 Max (ΔT°= 12 °C) than for p21 Max VL (ΔT°= 7 °C). This can be rationalized by a cooperative effect of DNA that is more prominent in the case of p21 Max. Indeed, we have shown elsewhere that the double mutation in the LZ had stabilized the HLH domain of Max*VL by a cooperative effect (*13*). In other words, if the probability of having the LZ domain folded was increased, this would in turn increase the probability of finding the HLH domain folded, hence, the cooperative stabilization. A similar effect can be expected on the HLH domain from the stabilization of the b-region. However, since the HLH domain of p21 Max VL is already stabilized by the double mutation, the cooperative stabilization coming from DNA is expected to be less important than in the case of p21 Max.

Finally, as can be observed in Figure 9, all of the p21 Max/E-Box dsDNA complex is denatured at 55 °C, while the p21 Max VL/E-Box dsDNA complex remains populated. The apparent increased stability of the protein/dsDNA interactions can therefore be linked to the higher probability of p21 Max VL of forming a dimer at higher temperature. Indeed, at 55 °C, no dimeric p21 Max exists at 32 μM, while most of the p21 Max VL is still dimeric (Supporting Information). Thus, the in vivo population of the p21 Max/E-Box dsDNA complex could be controlled either by its nuclear concentration or by the stability of its LZ domain.

DISCUSSION

On the basis of CD, NMR, sedimentation equilibrium, and velocity analytical ultracentrifugation, we show that, in absence of DNA, the HLH domain of p21 Max is stably folded but that its LZ domain is most likely undergoing a microscopic folding−unfolding transition in its dimeric state (Figure 11, vertical equilibrium on the left). The existence of the folding−unfolding transition of the LZ domain is

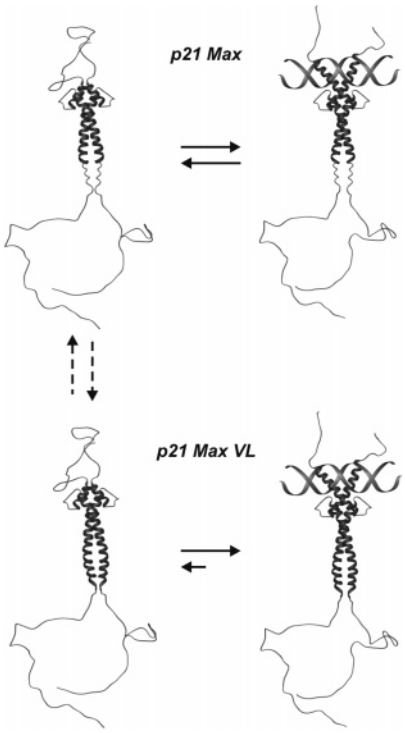

FIGURE 11: Microscopic folding−unfolding transition in the dimeric p21 Max and DNA binding. p21 Max is shown with its HLH domain folded and its LZ domain partially folded with both the N- and C-termini unstructured as suggested from CD, NMR, and AUC. Transient folding of the LZ domain of p21 Max (first vertical equilibrium) is shown to be quenched by the stabilizing N69V, H72L double mutation. As described in the text, this is supported by CD, NMR, and AUC. The stabilization of the LZ improves the stability of the p21 Max/E-Box complex (lower equilibrium).

further warranted by (1) a dramatic increase in stability, (2) a raise in α-helical content attaining that expected for a folded HLH-LZ, and (3) a concomitant elevation of the frictional ratio (increase in asymmetry) of the dimeric p21 Max VL construct (Figure 11). p21 Max VL was obtained by the N69V and H72L double mutation in the LZ domain of p21 Max. This demonstrates that the LZ domain of the p21 Max dimer is only transiently folded and further confirms that Asn69 and His72 are key residues in the destabilization of p21 Max, an integral part of the mechanism of specific heterodimerization (*29*−*31*).

Furthermore, our results demonstrate that neither the N-terminal nor the C-terminal domains are stably folded in the absence or in the presence of DNA (*23*). This clearly reveals that these regions do not structurally or directly contribute to homodimer formation or DNA binding. While it is known that a NLS is located in the C-terminal domain (*35*) and that phosphorylation sites are present in the N-terminal domain (*36*), our results raise the question about the existence of any structural function for the N- and C-terminal regions, which accounts for almost half of the protein. However, it has been shown that Max interacts with other proteins such as SMAD (*37*), Mnt (*38*), and Mga (*39*). It is possible that these regions of Max could undergo transient folding that may perhaps be stabilized by these proteins and play a role in the specific protein−protein interactions. This remains to be clarified.

We have determined an apparent K_D (37 °C) of 7.2×10^{-6} for p21 Max. To our knowledge, this is the first estimate of the K_D for the complete p21 gene product of Max. This value is markedly lower than the $(1-10) \times 10^{-5}$ values obtained for the isolated b-HLH-LZ domain at similar pH values (*13*, *26*). Interestingly, we demonstrate here that the b-HLH-LZ is destabilized by electrostatic repulsions. These repulsions are absent in p21 Max. Indeed, the thermodynamical stability of p21 Max is insensitive to ionic strength, while that of the b-HLH-LZ is highly sensitive. Interestingly, the N-terminus is very acidic, and its presence is known to reduce the positive and destabilizing electrostatic potential shown to exist at the interface of the HLH in absence of DNA (*20*). Therefore, the N-terminus could have an indirect or structurally passive role that could consist of reducing or masking these electrostatic repulsions present in the b-HLH-LZ in p21 Max and decrease its K_D to a physiologically functional range. It is still unclear whether Max homodimer play a role in transcription in vivo other than being the obligate partner of the Myc and Mad proteins. However, evidence suggests that, when overexpressed in cells, the Max homodimer can compete with c-Myc/Max heterodimer and reversibly repress transcription (*11*). However, the p21 Max homodimer can only play a role if it dimerizes in vivo. This has not been established before and will depend both on its K_D and its free concentration in the nucleus. While the nuclear concentration of Max has not been reported under any cellular state, it is estimated that 29 000 copies of c-Myc are present in the nucleus of proliferating fibroblasts (*40*). Assuming a volume of 5×10^{-10} cm^3 for the nucleus (*41*), the concentration of c-Myc in these cells is in the order of 1.5×10^{-7} M. Since p21 Max preferentially forms a heterodimer with c-Myc, its concentration in growing and proliferating cells must be, at the least, of the same order of magnitude. Given the observed K_D reported here (7×10^{-6}), it could be estimated that when c-Myc is down-regulated, the population of dimeric p21 Max, ready to bind DNA, should be in the order of 10%. The rest of the monomeric population would be poised to heterodimerize. It is noteworthy to remind that, when proliferating fibroblasts are treated with TGF-β, the level of c-Myc bound to Max decreases and the levels of Max and Mad proteins concomitantly increase (*12*). Moreover, after treatment with TGF-β, the amount of free Max significantly increases, possibly by a factor of 10 (*12*). Coupled to a down-regulation of c-Myc, this could lead to a transient increase in the population of dimeric Max, from 10 to 40%, assuming an increase in concentration from 1.5×10^{-7} to 1.5×10^{-6} M. Given that DNA binding will give rise to a mass action, one can safely assume that E-box sites originally occupied by the c-Myc-Max heterodimer could be transiently bound by the p21 Max dimer. While Max has not been demonstrated to interact with any co-activators or co-repressors, our results suggest that it could nevertheless transiently and reversibly represses the transcription of c-Myc target genes during the response to TGF-β. If the presence of TGF-β is maintained, the level of Mad will increase and most likely lead to heterodimerization between Mad and Max and the replacement of the p21 Max dimer on the E-box sites permanent repression of transcription by closure of the chromatin in the vicinity of the promoters. These estimates also depend on the nuclear concentrations of proteins of the Mad family and the relative affinities of these proteins for Max compared to the

thermodynamical stability of Max homodimers. This still has to be characterized.

Finally, the improved thermodynamical stability of the p21 Max VL construct over p21 Max that promotes the formation of significantly more E-Box complexes (Figure 11) at physiological concentrations could efficiently reduce the growth and proliferation of cancer cells that overexpress c-Myc. In this regard, p21 Max could have interesting applications in the study of cancer biology.

NOTE ADDED IN PROOF

Very recently, a gene expression profiling study of the crypt (proliferating cells)-villus (differentiated cells) axis of intestinal epithelial cells was published (*42*). This study reveals that Max is modestly expressed in the crypt cells but that it is expressed at a level exceeding those of Myc and Mad by at least 10-fold in the villus cells. Therefore, the Max homodimer should saturate the E-box sites in the villus cells (prevent binding of the c-Myc/Max heterodimers as discussed in our paper). This brings further support for a role of Max at repressing c-Myc functions.

ACKNOWLEDGMENT

The authors would like to thank Robert Eisenman for kindly providing plasmid pVZ1 containing the protein p21 Max. We are also grateful to the Queen's University Protein Function Discovery Facility for use of the AUC. Authors also want to thank Dr. Luc Tremblay for the expert NMR maintenance and for his help during the data acquisition.

SUPPORTING INFORMATION AVAILABLE

Thermodynamic charaterization of p21 Max and p21 Max VL and population plots. This material is available free of charge via the Internet at http://pubs.acs.org.

REFERENCES

1. Blackwood, E. M., and Eisenman, R. N. (1991) Max: a helix-loop-helix zipper protein that forms a sequence-specific DNA-binding complex with Myc, *Science 251*, 1211−1217.
2. Grandori, C., Cowley, S. M., James, L. P., and Eisenman, R. N. (2000) The Myc/Max/Mad network and the transcriptional control of cell behavior, *Annu. Rev. Cell Dev. Biol. 16*, 653−699.
3. Eberhardy, S. R., and Farnham, P. J. (2002) Myc recruits P-TEFb to mediate the final step in the transcriptional activation of the cad promoter, *J. Biol. Chem. 277*, 40156−40162.
4. Barsyte-Lovejoy, D., Mao, D. Y. L., and Penn, L. Z. (2004) c-Myc represses the proximal promoters of GADD45a and GADD153 by a post-RNA polymerase II recruitment mechanism, *Oncogene 23*, 3481−3486.
5. Peukert, K., Staller, P., Schneider, A., Carmichael, G., Hanel, F., and Eilers, M. (1997) An alternative pathway for gene regulation by Myc, *EMBO J. 16*, 5672−5686.
6. Staller, P., Peukert, K., Kiermaier, A., Seoane, J., Lukas, J., Karsunky, H., Moroy, T., Barket, J., Massague, J., Hanel, F., and Eilers, M. (2001) Repression of p15INK4b expression by Myc through association with Miz-1, *Nat. Cell Biol. 3*, 392−399.
7. Wanzel, M., Herold, S., and Eilers, M. (2003) Transcriptional repression by Myc, *Trends Cell Biol. 13*, 146−150.
8. Cowley, S. M., Kang, S. K., Frangioni, J. V., Yada, J. J., DeGrand, A. M., Radhakrishnan, I., and Eisenman, R. N. (2004) Functional analysis of the Mad1-mSin3A repressor-corepressor interaction reveals determinants of specificity, affinity, and transcriptional response, *Mol. Cell. Biol. 24*, 2698−2709.
9. Laherty, C. D., Yang, W. M., Sun, J. M., Davie, J. R., Seto, E., and Eisenman, R. N. (1997) Histone deacetylases associated with the mSin3 corepressor mediate mad transcriptional repression, *Cell 89*, 349−356.
10. Koskinen, P. J., Vastrik, I., Makela, T. P., Eisenman, R. N., and Alitalo, K. (1994) Max activity is affected by phosphorylation at two NH2-terminal sites, *Cell Growth Differ. 5*, 313−320.
11. Gu, W., Cechova, K., Tassi, V., and Dalla-Favera, R. (1993) Opposite regulation of gene transcription and cell proliferation by c-Myc and Max, *Proc. Natl. Acad. Sci. U.S.A.* 90, 2935−2939.
12. Siegel, P. M., Shu, W., and Massague, J. (2003) Mad upregulation and Id2 repression accompany transforming growth factor (TGF)-beta-mediated epithelial cell growth suppression, *J. Biol. Chem. 278*, 35444−35450.
13. Naud, J. F., Gagnon, F., Wellinger, R., Chabot, B., and Lavigne, P. (2003) Improving the thermodynamic stability of the leucine zipper of max increases the stability of its b-HLH-LZ:E-box complex, *J. Mol. Biol. 326*, 1577−1595.
14. Chen, Y. H., Yang, J. T., and Chau, K. H. (1974) Determination of the helix and beta form of proteins in aqueous solution by circular dichroism, *Biochemistry 13*, 3350−3359.
15. Kay L., Keifer, P., and Saarinen, T. (1992) Pure absorption gradient enhanced heteronuclear single quantum correlation spectroscopy with improved sensitivity, *J. Am. Chem. Soc. 114*, 10663−10665.
16. Weigelt, J. (1998) Single Scan, sensitivity- and gradient-enhanced TROSY for multidimensional NMR experiments, *J. Am. Chem. Soc. 120*, 10778−10779.
17. Delagio, F., Grzesieks, S., Vuister, G. W., Zhu, G., Pfeifer, J., and Bax, A. (1995) NMRPipe: a multidimensional spectral processing based on Unix pipes, *J. Biomol. NMR 6*, 277−293.
18. Johnson, B. A., and Blevins, R. A. (1994) NMRView: a computer program for the visualization and analysis of NMR data, *J. Biomol. NMR 4*, 603−614.
19. Schuck, P., Perugini, M. A., Gonzales, N. R., Howlett, G. J., and Schubert, D. (2002) Size-distribution analysis of proteins by analytical ultracentrifugation: strategies and application to model systems, *Biophys. J. 82*, 1096−111.
20. Sauve, S., Tremblay, L., and Lavigne P. (2004), The NMR solution structure of a mutant of the Max b/HLH/LZ free of DNA: insights into the specific and reversible DNA binding mechanism of dimeric transcription factors, *J. Mol. Biol. 342*, 813−832.
21. Nicholls, A., Sharp, K., and Honig, B. (1991) Protein folding and association: insights from the interfacial and thermodynamic properties of hydrocarbons, *Proteins 11*, 281−296.
22. Carson, M. (1997) Ribbons, *Methods Enzymol. 277*, 493−505.
23. Brownlie, P., Ceska, T. A., Lamers, M., Romier, C., Stier, G., Teo, H., and Suck, D. (1997) The crystal structure of an intact human Max−DNA complex: new insights into mechanisms of transcriptional control, *Curr. Biol.* 5, 509−520.
24. Ferre-D'Amare, A. R., Prendergast, G. C., Ziff, E. B., and Burley, S. K. (1993) Recognition by Max of its cognate DNA through a dimeric b/HLH/Z domain, *Nature 363*, 38−44.
25. Cohen, S. L., Ferre-d'Amare, A. R., Burley, S. K., and Chait, B. T. (1995) Probing the solution structure of the DNA-binding protein Max by a combination of proteolysis and mass spectrometry, *Protein Sci. 4*, 1088−1099.
26. Fieber, W., Schneider, M. L., Matt, T., Krautler, B., Konrat, R., and Bister, K. (2001) Structure, function, and dynamics of the dimerization and DNA-binding domain of oncogenic transcription factor v-Myc, *J. Mol. Biol. 307*, 1395−1410.
27. Krylov, D., Kasai, K., Echlin, D. R., Taparowsky, E. J., Arnheiter, H., and Vinson, C. (1997) A general method to design dominant negatives to B-HLHZip proteins that abolish DNA binding, *Proc. Natl. Acad. Sci. U.S.A. 94*, 12274−12279.
28. Horiuchi, M., Kurihara, Y., Katahira, M., Maeda, T., Saito, T., and Uesugi, S. (1997) Dimerization and DNA binding facilitate alpha-helix formation of Max in solution, *J. Biochem. 122*, 711−716.
29. Lavigne, P., Kondejewski, L. H., Houston, M. E., Jr., Sonnichsen, F. D., Lix, B., Sykes, B. D., Hodges, R. S., and Kay C. M. (1995) Preferential heterodimeric parallel coiled-coil formation by synthetic Max and c-Myc leucine zippers: a description of putative electrostatic interactions responsible for the specificity of heterodimerization, *J. Mol. Biol. 254*, 505−520.
30. Muhle-Goll, C., Nilges, M., and Pastore, A. (1995) The leucine zippers of the HLH-LZ proteins Max and c-Myc preferentially form heterodimers, *Biochemistry 34*, 13554−13564.
31. Lavigne, P., Crump, M. P., Gagne, S. M., Hodges, R. S., Kay, C. M., and Sykes, B. D. (1998) Insights into the mechanism of heterodimerization from the 1H-NMR solution structure of the c-Myc-Max heterodimeric leucine zipper, *J. Mol. Biol. 281*, 165−181.

32. Pervushin, K., Riek, R., Wider, G., and Wuthrich, K. (1997) Attenuated T2 relaxation by mutual cancellation of dipole−dipole coupling and chemical shift anisotropy indicates an avenue to NMR structures of very large biological macromolecules in solution, *Proc. Natl. Acad. Sci. U.S.A. 94*, 12366−12371.
33. Palmer, A. G., III, Kroenke, C. D., and Loria, J. P. (2001) Nuclear magnetic resonance methods for quantifying microsecond-to-millisecond motions in biological macromolecules, *Methods Enzymol. 339*, 204−238.
34. Palmer, A. G., III (2001) NMR probes of molecular dynamics: overview and comparison with other techniques, *Annu. Rev. Biophys. Biomol. Struct. 30*, 129−155.
35. Kato, G. J., Lee, W. M., Chen, L. L., and Dang, C. V. (1992) Max: functional domains and interaction with c-Myc, *Genes Dev. 6*, 81−92.
36. Bousset, K., Henriksson, M., Luscher-Firzlaff, J. M., Litchfield, D. W., and Luscher, B. (1993) Identification of casein kinase II phosphorylation sites in Max: effects on DNA-binding kinetics of Max homo- and Myc/Max heterodimers, *Oncogene 12*, 3211−3220.
37. Grinder, A. V., and Kerpola, T. (2003) Both Max and TFE3 cooperate with Smad proteins to bind the plasminogen activator inhibitor-1 promoter, but they have opposite effects on transcriptional activity, *J. Biol. Chem. 278*, 11227−11236.
38. Hurlin, P. J., Queva, C., and Eisenman, R. N. (1997) Mnt, a novel Max-interacting protein is coexpressed with Myc in proliferating cells and mediates repression at Myc binding sites, *Genes Dev. 11*, 44−58.
39. Hurlin, P. J., Steingrimsson, E., Copeland, N. G., Jenkins, N. A., and Eisenman, R. N. (1999) Mga, a dual-specificity transcription factor that interacts with Max and contains a T-domain DNA-binding motif, *EMBO J. 18*, 7019−7028.
40. Rudolph, C., Adam, G., and Simm, A. (1999) Determination of copy number of c-Myc protein per cell by quantitative Western blotting, *Anal. Biochem. 269*, 66−71.
41. Nair, S. K., and Burley, S. K. (2003) X-ray structures of Myc-Max and Mad-Max recognizing DNA. Molecular bases of regulation by proto-oncogenic transcription factors, *Cell 112*, 193−205.
42. Mariadason, J. M., Nicholas, C., L'Italien, K. E., Zhuang, M., Smartt, H. J. M., Heerdt, B. G., Yang, W., Corner, G. A., Wilson, A. J., Klampfer, L., Arango, D., and Augenlicht, L. H. (2005) Gene expression prolifing of intestinal epithelial cell maturation along the crypt-villus axis, *Gastroenterology 128*, 1081−1088.

BI0500729